공학석사 학위논문

The strategy for Acoustic full waveform inversion of Velocity and Density using l_1-norm

l_1-norm을 이용한 속도와 밀도의 음향파 완전 파형 역산 전략

2013년 2월

서울대학교 대학원

에너지시스템공학부

이 규 화

The strategy for Acoustic full waveform inversion of Velocity and Density using l_1-norm

l_1-norm을 이용한 속도와 밀도의 음향파 완전 파형 역산 전략

지도 교수 민 동 주

이 논문을 공학석사 학위논문으로 제출함
2012 년 12 월

서울대학교 대학원
에너지시스템공학부
이 규 화

이규화의 공학석사 학위논문을 인준함
2013 년 1 월

위 원 장 _____ (인)

부위원장 _____ (인)

위 원 _____ (인)

ABSTRACT

Full waveform inversion (FWI) is one of the seismic data processing methods, which plays a key role in imaging subsurface structures and getting information of physical properties of target media. There are many studies that obtain successful results from elastic waveform inversion with multi parameters. However, when it comes to real field data, the acoustic FWI can be preferred because of computational overburden. Conventional acoustic FWI has been performed only with P-wave velocity under the assumption that density is constant or media are hydrostatic. However, in real earth media, density is not constant and media are not hydrostatic. Realizing that density is important in oil and gas exploration, there have been attempts to estimate density from FWI.

In this thesis, we propose an acoustic FWI strategy that can estimate both velocity and density information based on the l_1 –norm objective function. Our inversion strategy consists of two stages and uses the two different parameterizations of acoustic wave equation that support heterogeneous media. One is parameterized with the bulk modulus and the density (Type-1). And the other is with the velocity and the density (Type-2). Type-1 yields better results in velocities than Type-2, while Type-2 gives more reliable density information than Type-1. The bulk modulus is first inverted while density is fixed at a constant value and the velocity is reconstructed through relationship between the bulk modulus and the density. Next, velocity and density are simultaneously inverted based on velocity results obtained in the first stage. Velocity is updated using the gradient direction of the bulk modulus through the chain rule. The inversion strategy applied to noise-free and noise-added. Synthetic data for the SEG/EAGE overthrust model. As a result, we were able to obtain reliable results for both velocity and density in both cases of noise-free and noise-added data.

KEYWORDS: acoustic, waveform inversion, frequency-domain, density inversion

STUDENT NUMBER: 2011-21105

CONTENTS

LIST OF FIGURES

1. INTRODUCTION

Full waveform inversion (FWI) is a promising method to estimate physical properties of subsurface media from field data. Because of the significant role of FWI, it has been widely researched and developed in numerous studies. However, it still has several problems to be overcome in order to be applied to real field data. In particular, elastic and anisotropic FWIs suffer from computational overburden and instability between some parameters. In addition, 3-D FWI can only be conducted under the assumption that subsurface media are acoustic and isotropic. For these reasons, FWI has mainly been conducted with acoustic wave equation, assuming that subsurface media are acoustic and isotropic in practical field.

In conventional acoustic FWI, only P-wave velocity has usually been inverted. However, density information is also required to accurately interpret subsurface media in oil and gas exploration. There were several attempts to recover density information but they only confirmed that density is difficult to recover from FWI (Forgues and Lambare, 1997; Virieux and Operto, 2009).

In this thesis, we propose the strategy for acoustic FWI that can yield reasonable results for both velocity and density information based on the method suggested by Jeong *et al.* (2012) for the elastic FWI.

The inversion strategy is composed of two stages and it uses a different parameterization of heterogeneous acoustic wave equation in each stage. Bulk modulus is recovered in the first stage, fixing density at a random constant value for the entire model. Velocity can be extracted from bulk modulus and density. Although the inverted bulk modulus and density are not correct, the velocity can be compatible with true value. In the second stage, both velocity and density are simultaneously inverted using velocity information obtained in the first stage as initial guess for the velocity.

For forward modeling and inversion algorithm, the finite-element method (Zienkiewicz and Taylor, 2000) is applied to demonstrate wave propagation. The objective function is based on l_1-norm that has been robust for noisy data (Pyun *et al.*, 2009). The gradient method (Lailly,

1983; Tarantola, 1984; Pratt et al., 1998) is used to update model parameters. The conjugate gradient method (Fletcher & Reeves 1964) is applied to accelerate convergence rate of inversion. Pseudo-Hessian (Shin *et al*., 2001) and the random phase-encoded simultaneous-source method (Romero et al., 2000; Krebs et al., 2009; Ben-Hadj-Ali *et al*., 2011) are employed to achieve computation efficiency. Inversion strategy is demonstrated for the SEG/EAGE overthrust model. In order to check the feasibility of the strategy for real field data, we applied the acoustic FWI with the new strategy to data with outliers.

2. INVERSE THEORY

2.1. Objective function and gradient method

Seismic waveform inversion is the technique designed to delineate material properties of subsurface structure. It is performed in the way of minimizing the difference between modeled data and observed data.

The objective function is defined to measure differenced between modeled data and field data. The objective function based on the l_1-norm can be expressed (Pyun *et al*., 2007) as,

$$E(\mathbf{p}) = \sum_{i=1}^{n_s}\sum_{j=1}^{n_r}\left\{\left|\mathrm{Re}\left[u_{ij}(\mathbf{p}) - d_{ij}\right]\right| + \left|\mathrm{Im}\left[u_{ij}(\mathbf{p}) - d_{ij}\right]\right|\right\}, \quad (1)$$

where $u_{ij}(\mathbf{p})$ and d_{ij} indicate modeled data and field data, respectively. n_s and n_r are total number of sources and receivers, respectively, and the subscripts i and j are source and receiver indices.

Gradient method is used to minimize the objective function. In this case, model parameter ($\mathbf{p}$) can be updated as follows,

$$\mathbf{p}^{t+1} = \mathbf{p}^{t} - \alpha \nabla_p E^t, \quad (2)$$

where t is the number of iteration, and α indicates the step length. The gradient of $E(\mathbf{p})$ will give the direction where l_1-norm increases in the fastest rate, and by taking negative direction in front of it, the objective function will be always reduced until it reaches the convergence area.

The gradient direction can be obtained by taking partial derivatives of eq. (1) with respect to the k^{th} model parameter, which yields,

$$-\nabla_{p_k} E(\mathbf{p}) = -\mathrm{Re}\left[\sum_{i=1}^{n_s}\sum_{j=1}^{n_r}\frac{\partial u_{ij}(\mathbf{p})}{\partial p_k}\overline{\left\{\mathrm{sgn}\left(\mathrm{Re}\left[u_{ij}(\mathbf{p}) - d_{ij}\right]\right) + i\,\mathrm{sgn}\left(\mathrm{Im}\left[u_{ij}(\mathbf{p}) - d_{ij}\right]\right)\right\}}\right]. \quad (3)$$

In this thesis, rather than directly calculating partial derivatives from above eq. (3), the gradient is obtained by using the back propagation. This method

has been widely used for reverse-time migration (Pratt *et al*. 1998 ; Shin & Min 2006).

In the frequency domain, forward modeling can be computed solving the matrix equation expressed by,

$$\mathbf{Su} = \mathbf{f} \,, \tag{4}$$

where $\mathbf{S}$ indicates the complex impedance matrix and $\mathbf{f}$ is the source vector.

This method starts with taking partial derivatives of complex impedance matrix of forward modeling with respect to the k^{th} model parameter:

$$\frac{\partial \mathbf{S}}{\partial p_k}\mathbf{u} + \mathbf{S}\frac{\partial \mathbf{u}}{\partial p_k} = 0 \,, \tag{5}$$

$$\frac{\partial \mathbf{u}}{\partial p_k} = \mathbf{S}^{-1}\left(-\frac{\partial \mathbf{S}}{\partial p_k}\mathbf{u}\right) = \mathbf{S}^{-1}\mathbf{f}_k^v \,, \tag{6}$$

where $\mathbf{f}_k^v$ is virtual source for the k^{th} parameter. Jacobian matrix test is performed in order to verify forward modeling algorithm by comparing partial derivatives and analytic solution of it and it can be referred in Appendix A.

By substituting the partial derivative wavefield in eq. (3) with eq. (6), we can obtain the gradient at the k^{th} parameter in following form:

$$\nabla_{p_k} E(\mathbf{p}) = \mathrm{Re}\left[\sum_{i=1}^{n_s}\sum_{j=1}^{n_r}\left(\mathbf{f}_k^v\right)^T\left(\mathbf{S}^{-1}\right)^T r_{ij}\right], \tag{7}$$

where T means the transpose, and r_{ij} is given by,

$$r_{ij} = \overline{\mathrm{sgn}\left(\mathrm{Re}\left[u_{ij}(\mathbf{p}) - d_{ij}\right]\right) + \mathrm{i}\,\mathrm{sgn}\left(\mathrm{Im}\left[u_{ij}(\mathbf{p}) - d_{ij}\right]\right)}. \tag{8}$$

In eq. (7), $\left(\mathbf{S}^{-1}\right)^T r_{ij}$ indicates the backpropagated residual.

When it comes to the step of scaling gradient which enhances images of inversion results, the approximate Hessian can be used in Gauss-Newton

method. However, computing the approximate Hessian matrix causes computational overburden. To overcome this computational problem, Shin *et al*. (2001) suggested the pseudo-Hessian which is computed by using virtual sources of model parameters and it can be expressed for all model parameters as below,

$$\nabla E(\mathbf{p}) = \left(\sum_{i=1}^{n_s} \left(\mathbf{F}_i^* \right)^T \mathbf{F}_i^* + \beta \mathbf{I} \right)^{-1} \mathrm{Re} \left[\sum_{i=1}^{n_s} \left(\mathbf{F}_i^* \right)^T \mathbf{S}^{-1} \mathbf{r}_i \right], \tag{9}$$

where β and $\mathbf{I}$ indicate the damping factor that is added to avoid singularity problem and unit vector respectively, and * means conjugate transpose. $\mathbf{F}_i^*$ and $\mathbf{r}_i$ are,

$$\mathbf{F}_i^* = \left[\mathbf{f}_{i1}^* \;\; \mathbf{f}_{i2}^* \;\; \dots \;\; \mathbf{f}_{ik}^* \;\; \dots \;\; \mathbf{f}_{in_p}^* \right], \tag{10}$$

$$\mathbf{r}_i = \left[\mathrm{r}_{i1} \;\; \mathrm{r}_{i2} \;\; \dots \;\; \mathrm{r}_{in_r} \;\; 0 \;\; \dots \;\; 0 \right]^T. \tag{11}$$

In order to increase convergence rate of inversion, conjugate gradient method is applied in this research that was suggested by Fletcher et al. in 1964. In this case, final gradient direction (g) can be obtained as follows,

$$\mathbf{p}^{l+1} = \mathbf{p}^l + \alpha g^l, \tag{12}$$

$$g^l = -\nabla_p E^l + \frac{\left(\nabla_p E^l \right)^T \nabla_p E^l}{\left(\nabla_p E \right)^T \nabla_p E^{T-1}} g^{l-1}. \tag{13}$$

2.2. Simultaneous sources technique

In the frequency domain, as we did earlier, wave equation can be expressed with matrix as below

$$\mathbf{Su} = \mathbf{f} \ . \tag{14}$$

The gradient can be calculated by adjoint-state method. In frequency domain, the gradient at one source and one frequency is obtained by multiplication between the wavefield (eq. 15) which is gotten from that source, the residual wavefield (eq. 16) which is back-propagated and the matrix that taken partial differentiated by the model parameter (eq. 17).

$$\mathbf{u}_{ij} = \mathbf{S}_i^{-1}\mathbf{f}_{ij} \tag{15}$$

$$\mathbf{r}_{ij}^{*} = \mathbf{S}_i^{-1}\mathbf{u}_{ij}^{*} \tag{16}$$

$$\mathbf{u} = \frac{\partial \mathbf{S}}{\partial \mathbf{P}} \tag{17}$$

When we use multiple sources, we can express the gradient on the parameter (p_l) at a frequency (i) as

$$\left(\frac{\partial E(\mathbf{p})}{\partial p_l} \right)_i = \sum_{j=1}^{N_s} \mathbf{u}_{ij}^T \mathbf{S}_{il}^T \mathbf{r}_{ij}^{*} \ . \tag{18}$$

The simultaneous-shot technique is the efficient method that can reduce the amount of computation in migration and waveform inversion. It reduces the number of wave simulation by summing supershot($\mathbf{s}$) using linear relationship between seismic wavefield and source as follows,

$$\overline{\mathbf{s}} = \sum_{j=1}^{N_s} a_j \mathbf{s}_j \ . \tag{19}$$

And $\overline{\mathbf{p}}$ and $\overline{\mathbf{r}}$ can be expressed in the form of supershot and be written as

$$\bar{\mathbf{p}} = \sum_{j=1}^{N_s} a_j \mathbf{p}_j \quad , \tag{20}$$

$$\bar{\mathbf{r}}^* = \sum_{j=1}^{N_s} a_j^* \mathbf{r}_j^* \quad , \tag{21}$$

where a_j indicate $\exp\left(i\phi_j\right)$ when i is $\sqrt{-1}$.

In this manner, the gradient can be expressed as

$$\left(\frac{\partial E(\mathbf{p})}{\partial p_l}\right)_i = \sum_{j=1}^{N_s}\sum_{k=1}^{N_s} a_{ij} a_{ik}^* \mathbf{u}_{ij}^T \mathbf{S}_{il}^T \mathbf{r}_{ik}^* = \sum_{j=1}^{N_s} \mathbf{u}_{ij}^T \mathbf{S}_{il}^T \mathbf{r}_{ij}^* + \sum_{j=1}^{N_s}\sum_{\substack{k=1 \\ k\neq j}}^{N_s} a_{ij} a_{ik}^* \mathbf{u}_{ij}^T \mathbf{S}_{il}^T \mathbf{r}_{ik}^* \,. \tag{22}$$

The second term in right side of the formula is crosstalk noise between source j and k, and can be minimized through phase function ($\exp\left(i\phi_j\right)$).

3. INVERSION STRATEGY FOR DENSITY

3.1. 2D frequency-domain acoustic wave equation

In heterogeneous and isotropic media , the 2-D acoustic wave equation can be written as

$$-\frac{\omega^2}{K}\tilde{p}=\frac{\partial}{\partial x}\left(\frac{1}{\rho}\frac{\partial \tilde{p}}{\partial x}\right)+\frac{\partial}{\partial z}\left(\frac{1}{\rho}\frac{\partial \tilde{p}}{\partial z}\right) \tag{23}$$

where ω is angular frequency, K and ρ represent the bulk modulus and the density, respectively, and $\tilde{p}$ is the pressure wavefield in frequency-domain. It can also be parameterized with terms of P-wave velocity and density as below

$$-\frac{\omega^2}{v_p^2\rho}\tilde{p}=\frac{\partial}{\partial x}\left(\frac{1}{\rho}\frac{\partial \tilde{p}}{\partial x}\right)+\frac{\partial}{\partial z}\left(\frac{1}{\rho}\frac{\partial \tilde{p}}{\partial z}\right). \tag{24}$$

And we can express these equations in the form of matrix-vector with vertical source vector as eq. (3), applying finite elements concepts which employ Galerkin method (Zienkiewicz and Taylor, 2000),

$$\left(\frac{1}{\rho}\left(\mathbf{K}_{xx}+\mathbf{K}_{zz}\right)-\frac{\omega^2}{K}\mathbf{M}\right)\tilde{u}=\tilde{f}, \tag{25}$$

$$\left(\frac{1}{\rho}\left(\mathbf{K}_{xx}+\mathbf{K}_{zz}\right)-\frac{1}{\rho}\frac{\omega^2}{v_p^{\,2}}\mathbf{M}\right)\tilde{u}=\tilde{f}. \tag{26}$$

where $\mathbf{K}_{xx}$ and $\mathbf{K}_{zz}$ indicate horizontal and vertical direction of stiffness matrix, respectively and $\mathbf{M}$ is mass matrix in acoustic media.

Even though two wave equations described above are parameterized differently, their complex impedance matrices of them are the same. In order to check it, forward modeling is conducted on each parameterization with SEG/EAGE overthrust model. And wavefield traces are compared in time domain. It can be checked in Figure 1 shown as follow.

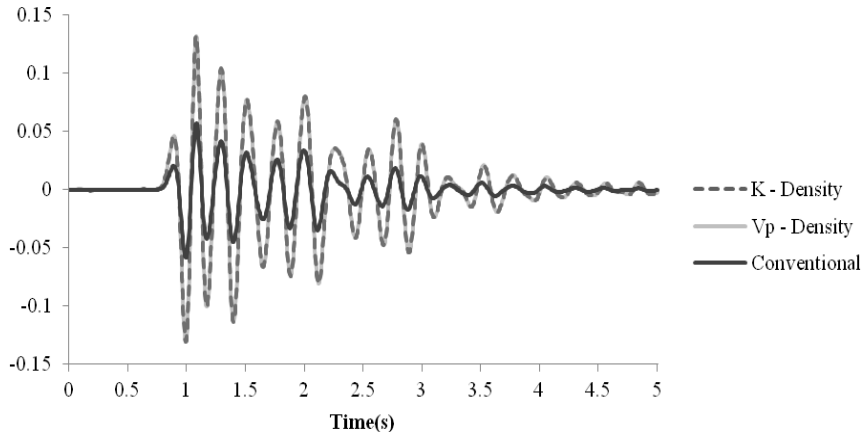

Figure 1 Comparison on traces of wavefield in time-domain between parameterization in acoustic wave equation. Dotted line and grey line indicate K-density parameterization and V_p-density parameterization. And solid line shows conventional parameterization.

Dotted line and grey line indicate wavefield plots of eq. (23) and eq. (24) generated in time domain at the location of 4.35 km and 261-th shot respectively. In addition to it, conventional acoustic wave equation which does not consider density by assuming density as constant value for entire modeling region is compared to wave equations of eq. (23) and eq. (24) in order to see the difference between the cases, the ones which actually consider density and the other case which does not. It can be seen conventional acoustic wave equation, solid line, does not seem to be able to show the effect of density. It is only propagating differently while the eq. (23) and eq. (24) wave equations' plots are exactly the same. It indicates that density can be important in seismic modeling and inversion.

3.2. 2D frequency-domain acoustic inversion

As mentioned earlier, extracting reasonable information of velocity and density at the same time was unsuccessful. For this reason, hierarchical inversion strategy is proposed in this thesis. Since it is hard to get velocity and density simultaneously, it is reasonable to estimate each physical property hierarchically, applying each of two parameterization methods in each stage. In our inversion strategy, velocity and density are recovered over two stages. In first stage, P-wave velocity is gotten since it is known that velocity information can be recovered well even with wrong density information as it does in conventional acoustic full waveform inversion. In second stage, density is estimated based on velocity obtained in the first stage. In this stage, velocity is also updated. For convenience, acoustic wave equations shown in eq. (23) and (24) will be called as parameterization 'Type-1 (the bulk modulus and the density)' and 'Type-2 (the velocity and the density)' respectively from now.

First, velocity is inverted with density fixed at a constant value in order to investigate which parameterization yields better result. In case of Type-1, since it is parameterized as the bulk modulus and the density, we first invert the bulk modulus and obtain velocity information by the relation between the bulk modulus and the density. In our experiment, both Type-1 and Type-2 recover the velocity well but Type-1's result seems to be slightly better than one from Type-2, tracking velocity information more smoothly. Velocity information obtained by Type-2 shows some over estimated parts. Type-1 and Type-2 yield different inversion results because their virtual sources are different, which are used to compute the gradient direction. By taking partial derivative of eq. (25) and eq. (26) with respect to the bulk modulus and velocity, respectively, virtual source of the bulk modulus from Type-1 and the one of velocity from Type-2 can be expressed as,

$$\mathbf{S}\frac{\partial \tilde{u}}{\partial K} = -\frac{\omega^2}{K^2}(\mathbf{M})\tilde{u}\,, \tag{27}$$

$$\mathbf{S}\frac{\partial \tilde{u}}{\partial v_p} = -\frac{\omega^2}{v_p{}^3\rho}(\mathbf{M})\tilde{u}\,. \tag{28}$$

Type-2 virtual source for velocity has density term. So it can be affected by wrongly assumed density information. Meanwhile, Type-1 estimates the

velocity indirectly, inverting the bulk modulus. The relationship between the bulk modulus and density which results in the velocity can be expressed as

$$v_p = \sqrt{\frac{K_{\mathrm{v}}}{\rho_{\mathrm{c}}}}, \tag{29}$$

where K_{v} and ρ_{c} indicate virtual bulk modulus and the density with constant value. Consequently, Type-1 is more suitable to invert the velocity in first stage.

In the case of density, it is also investigated which parameterization yields better result, assuming true velocity model is known to see only the performance of each Type's virtual source of the density, with synthetic true model as SEG/EAGE overthrust. The overthrust model is modified with removing some parts of sides and bottom. The density model is made with empirically derived equation suggested by Gardner *et al.* (1974). The equation that relates seismic P-wave velocity to the bulk density of the lithology in which the wave travels and widely used in petroleum exploration because it can provide information about the lithology from interval velocities obtained from seismic data. Figure 2 shows velocity and density models of the SEG/EAGE overthrust model. The dimension of the model is 12 km × 4 km with a grid interval of 0.025 km. For boundary condition, Perfect matched layers (PML) is employed and it needs additional 20 grid points each on both sides and the bottom by extending the original model. In this way, the number of grid points of modeling is 521 in width and 181 in depth. Sources are excited at 241 points except in boundary condition region with an interval of 0.05 km, while receivers are placed at all the surface grid points except the boundary region. For source wavelet, the first derivative of the Gauss function which has maximum frequency of 10 Hz is used with the maximum recording time of 5 seconds.

Figure 3 shows inversion results of velocities obtained at the 1000-th iteration when the density is fixed at 2.3 $\mathrm{g/cm^3}$. Both Type-1 and Type-2 show generally good results but some artifacts at high frequency are detected in Type-2. Also depth profiles of Type-1, Type-2 and true model are compared in Figure 4. In Figure 4, Type-2 over estimated true model in several parts when Type-1 shows more stable plot.

For density, we performed as linear increasing model ranging from 2.158 to 2.725 $\mathrm{g/cm^3}$. We assumed that velocity is known. The density inversion

results at 500-th iteration are shown in Figure 5. We may feel that Type-2 looks closer to the true model than Type-1. From depth profiles shown in Figure 6, however, both parameterizations do not recover density well even with the information of true velocity model. But in shallow depth, Type-1 tends to estimate the density out of the true density model and is more deviated from true model than Type-2 overall. Hence, Type-2 can be more suitable to restore density in second stage. This is because Type-1 and Type-2's virtual sources for density are different. Virtual sources for density from Type-1 and Type-2 can be obtained by taking partial derivative of eq. (25) and eq. (26) respect to density and it can be written as,

$$\mathbf{S}\frac{\partial \tilde{u}}{\partial \rho} = \frac{1}{\rho^2}\left(\mathbf{K}_{xx} + \mathbf{K}_{zz}\right)\tilde{u}\,, \tag{30}$$

$$\mathbf{S}\frac{\partial \tilde{u}}{\partial \rho} = \left(\frac{1}{\rho^2}\left(\mathbf{K}_{xx} + \mathbf{K}_{zz}\right) - \frac{1}{\rho^2}\frac{\omega^2}{v^2}\mathbf{M}\right)\tilde{u}\,. \tag{31}$$

As in the case of velocity, virtual source of the density in Type-2 has velocity term in its formula and this supports better density results by generally well recovered velocity in acoustic FWI

Consequently, we use Type-1 parameterization in the first stage to obtain the velocity and Type-2 in second stage for the density using the velocity result obtained in the previous stage. In the second stage, when we update the velocity rather than just using virtual source of the velocity from Type-2, virtual source of the bulk modulus from Type-1 better to be used which is more stable than Type-2 in getting velocity information as shown in Figure 3 and 4, applying chain rule to convert the gradient of the velocity into the bulk modulus as Jeong *et al*. (2012) did in the case of elastic FWI. It can be expressed as,

$$\frac{\partial \mathbf{u}}{\partial K} = \mathbf{S}^{-1}\left\{-\left(\frac{\partial \mathbf{S}}{\partial v_p}\frac{\partial v_p}{\partial K} + \frac{\partial \mathbf{S}}{\partial \rho}\frac{\partial \rho}{\partial K}\right)\mathbf{u}\right\}. \tag{32}$$

(a)

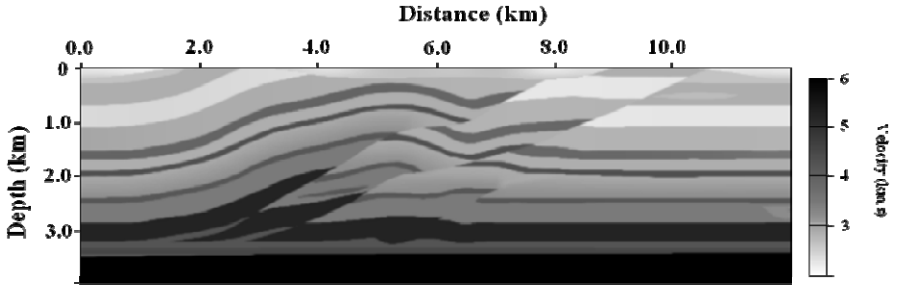

(b)

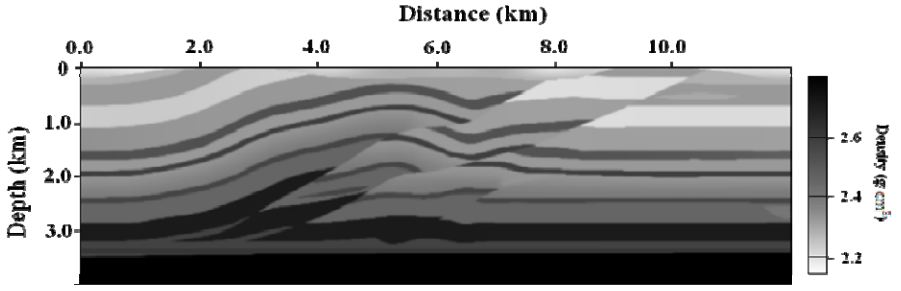

Figure 2 The SEG/EAGE overthrust true model of (a) P-wave velocity and (b) density.

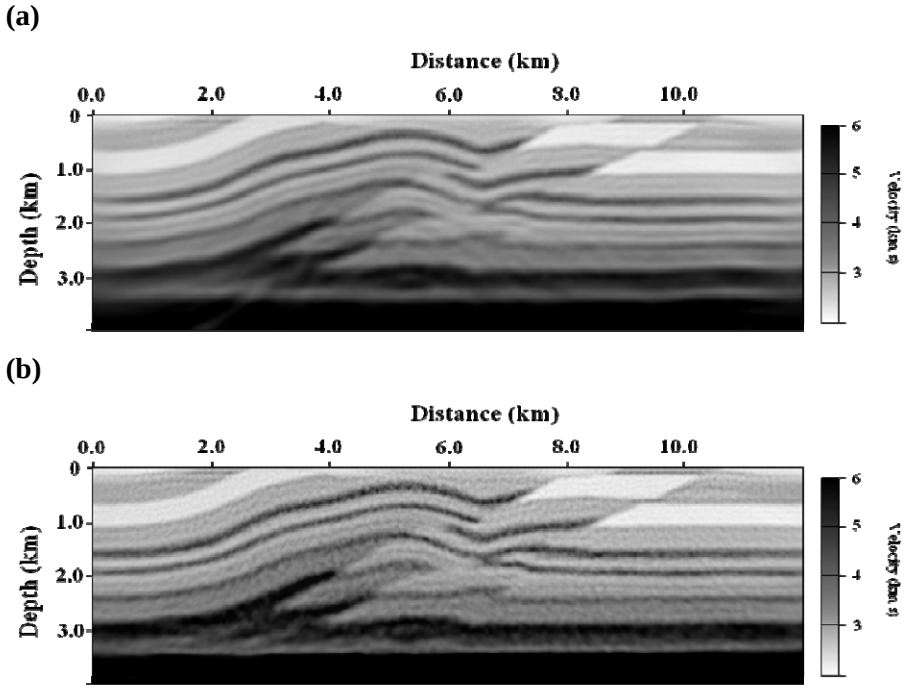

Figure 3 Velocity models inverted in the 1000-th iteration by (a) Type-1 and (b) Type-2 parameterizations, fixing density at a constant value for the entire model.

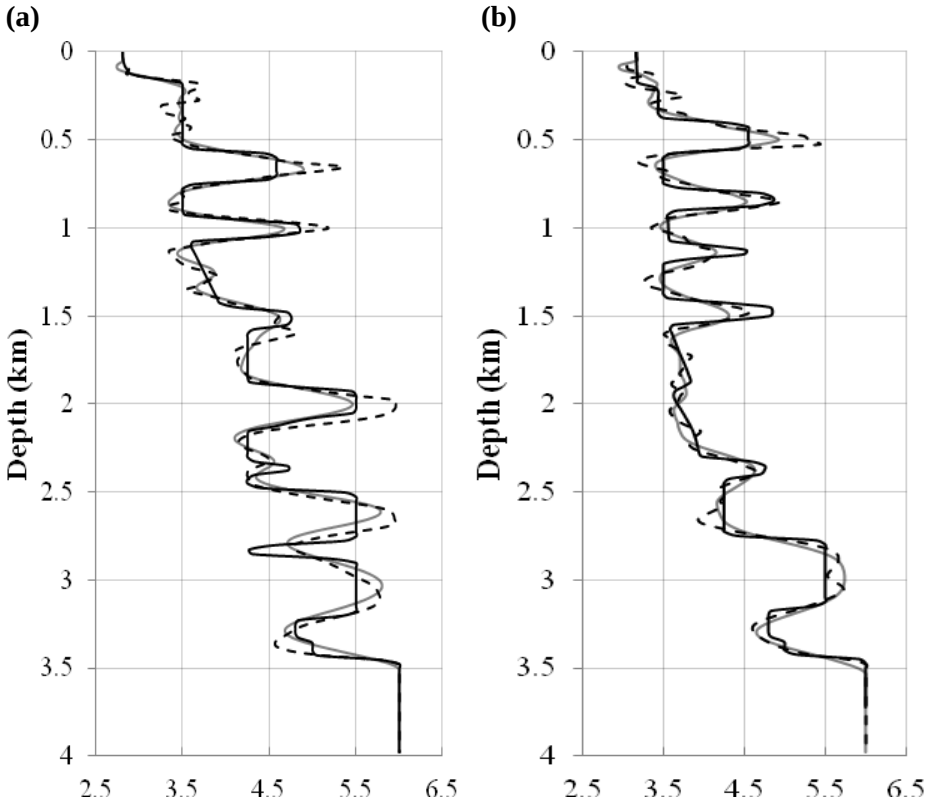

Figure 4 Depth profiles extracted at distances of (a) 4km and (b) 6km of inverted velocity (Figure 3) and true velocity models. Grey solid and black dashed lines indicate Type-1 and Type-2, respectively, and black solid line indicates true velocity model. The unit of velocity is km/s.

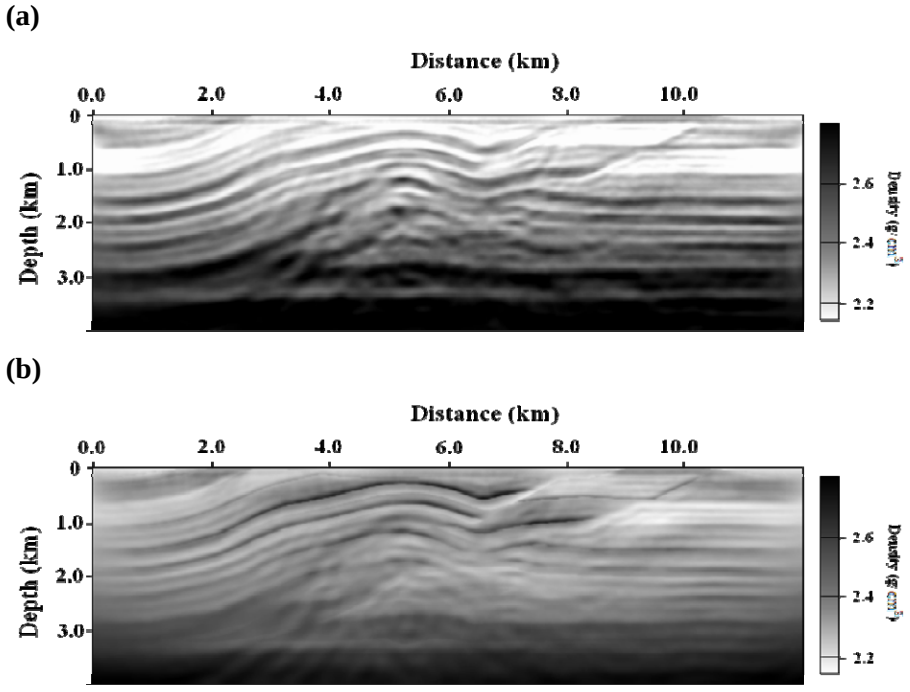

Figure 5 Density models inverted in the 500-th iteration by (a) Type-1 and (b) Type-2, assuming that true velocity model is known.

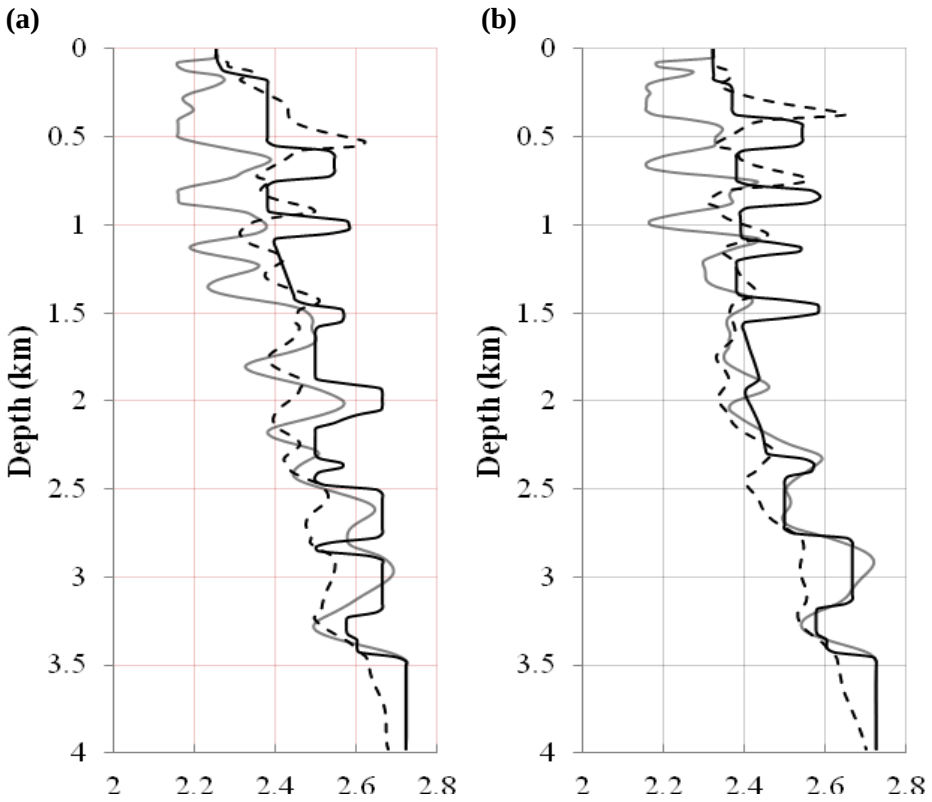

Figure 6 Depth profiles extracted at distances of (a) 4km and (b) 6km of inverted density (Figure 5) and true velocity models. Grey solid and black dashed lines indicate Type-1 and Type-2, respectively, and black solid line indicates true density model. The unit of density is g/cm^3.

4. NUMERICAL EXAMPLES

We demonstrate our inversion strategy for the same SEG/EAGE overthrust model. We first apply the inversion strategy for noise-free data. To investigate the feasibility of our strategy for noisy field data, we apply the inversion strategy for noise-added data. Figure 7 shows noise-free and noise-added seismograms generated for the SEG/EAGE overthrust model. For noise, outlier, spike noise, is chosen whose amplitude is 5 times bigger than the maximum value of the trace at randomly chosen 5 different frequencies and locations.

In the first stage, FWI is conducted only for velocity with density fixed at 2.3 g/cm^3, randomly chosen in reasonable range of density values. A linear increasing model is used for initial guess which ranges from 2.36 to 6.00 km/s. Inversion result is shown in Figure 8 and it has very good estimation of real structures.

For the second stage inversion, the velocity information obtained in the first stage is used as initial guess for the velocity and a linear increasing model ranging from 2.158 to 2.725 g/cm^3 is used for density. Figure 9 shows finally reconstructed inversion results of both velocity and density in the 2000-th iteration. Figure 9 shows that density recovered by the inversion strategy is better than those restored by the conventional way that inverts velocity and density simultaneously. Also in depth profiles shown in Figure 10 and 11, not only P-wave velocity but also the density tracks down structures of true model well.

As mentioned earlier, we also added some noises artificially on forward modeling data and performed FWI with our inversion strategy. Figure 12 shows inverted velocity in the same way as we did in the case without noises and it looks very reasonable and close to true model. Velocity and density are inverted simultaneously in the same way that uses inverted velocity information obtained in the first stage and set initial guess for the density as linear increasing model with the same range as the noise-free case. Even when noises are added, we can note that our inversion strategy shows satisfactory results, showing low sensitivity to factors that can affect inversion results such as noises (Figure 13, 14, and 15).

Comparisons have been made between the cases: one without noises and the other one is noise-added. Both of them show good results in both velocity and density (Figure 16 and 17). Despite in the case of the density (Figure 17), it can be seen there are some parts where the one with noises is a little more

deviated from true model than the one without noises but overall both cases track true model moderately well.

By employing simultaneous sources technique for computation efficiency, we iterated 1500 times of updating process in first stage which took only about 3200s. And in second stage, it took about 4300s with 2000 times of iteration using 20 Intel Xeon E5640 2.66 GHz CPUs on the Linux-cluster machine.

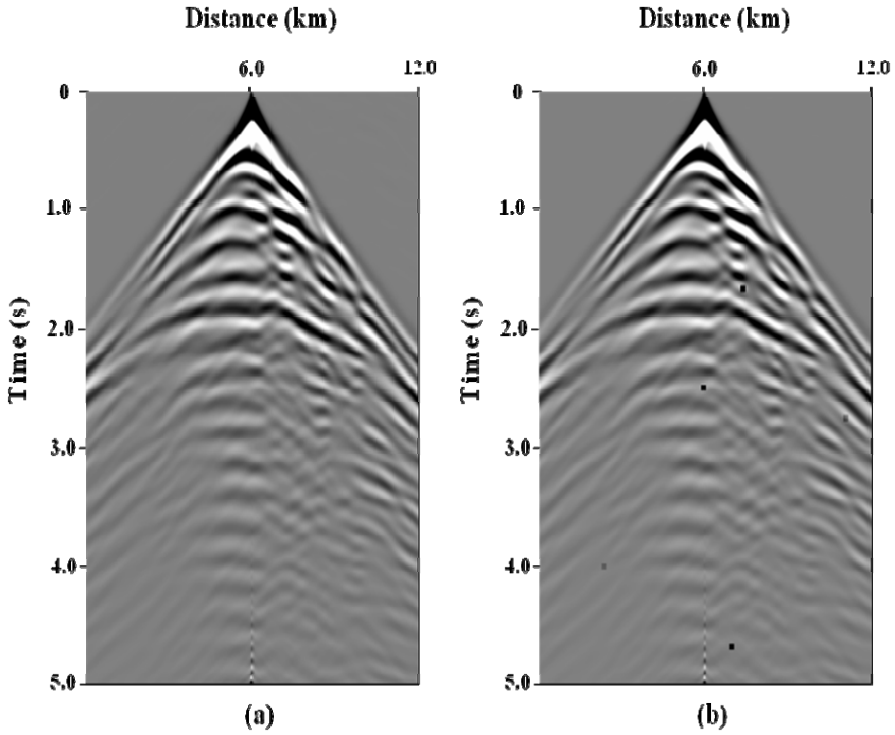

Figure 7 Synthetic seismograms of displacements obtained from forward modeling on SEG/EAGE overthrust model: (a) without noises, (b) noises added

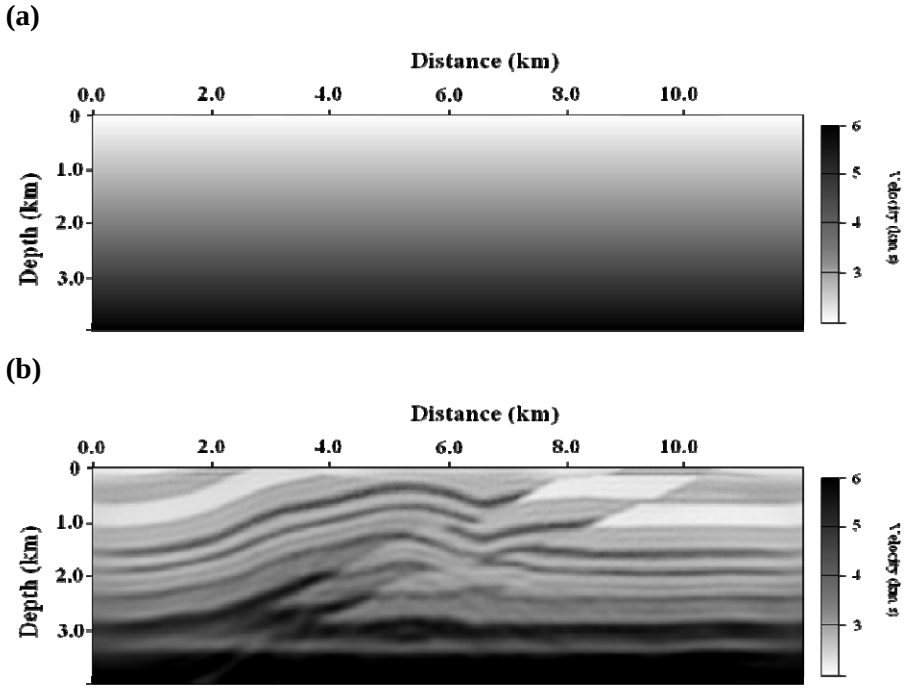

Figure 8 The initial guess (a) and first stage inversion result of the velocity at 1500-th iteration shown in (b). The density is fixed as constant value for whole modeling region.

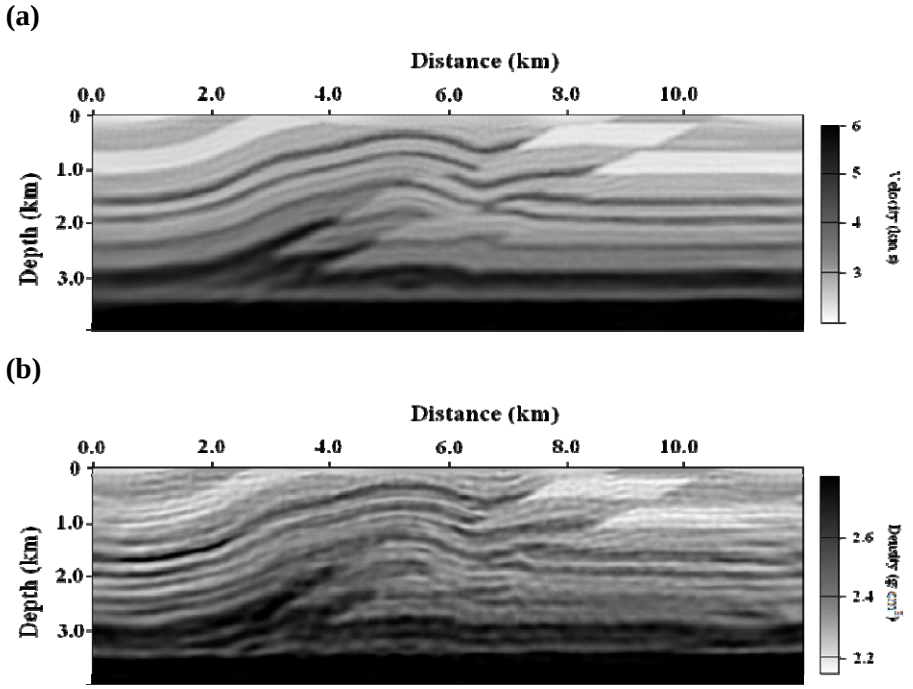

Figure 9 The final results of velocity and density in the 2000-th iteration for (a) P-wave velocity and (b) density.

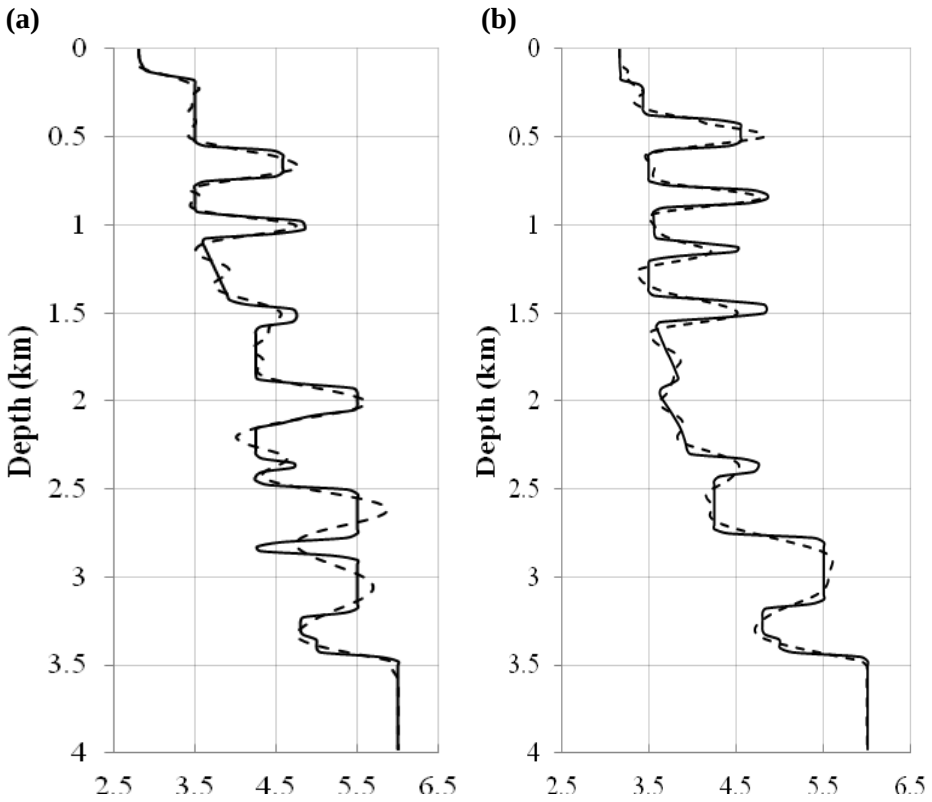

Figure 10 The final inversion results of depth profiles obtained from the velocity model which is shown in Figure 9-(a) at the location of (a) 4km and (b) 6km. Dashed line and black line indicate inverted P-wave velocity and true model. The unit of velocity is km/s.

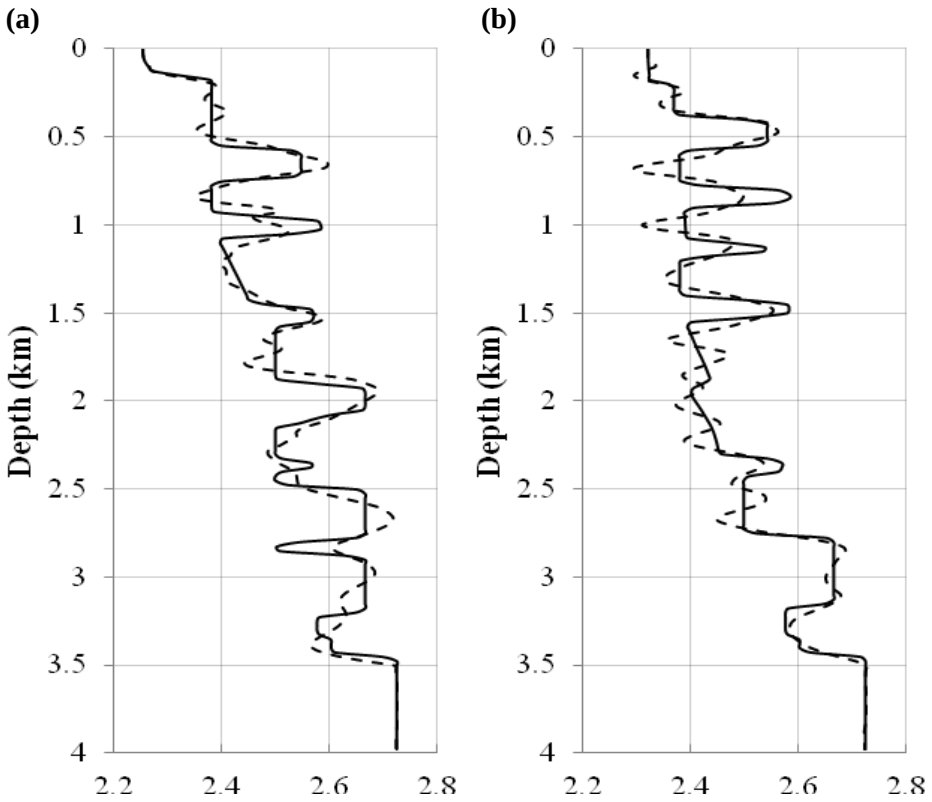

Figure 11 The final inversion results of depth profiles obtained from the density model which is shown in Figure 9-(b) at the location of (a) 4km and (b) 6km. Dashed line and black line indicate inverted the density and true model. The unit of density is g/cm^3.

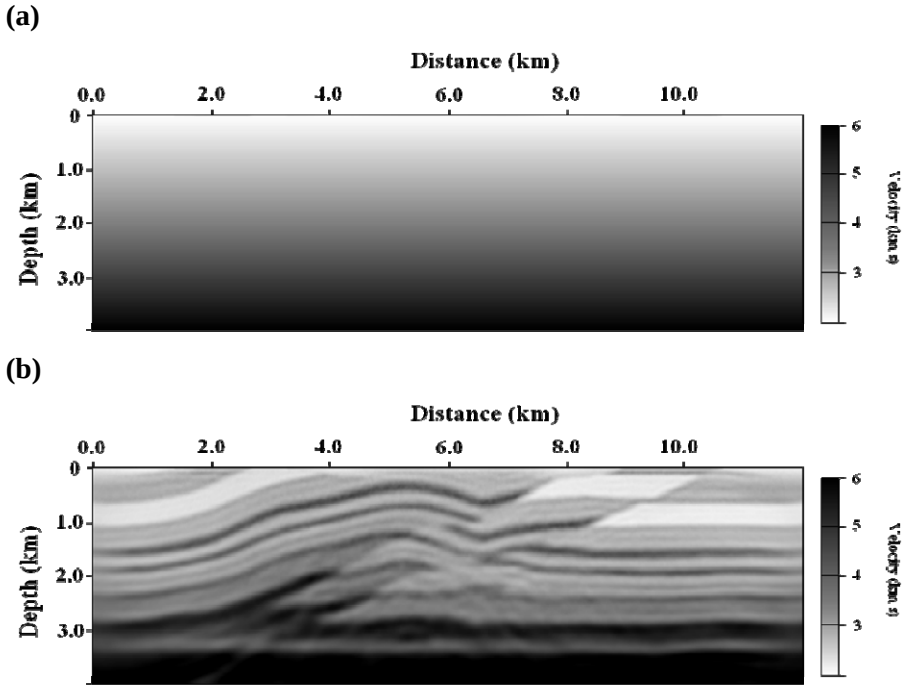

Figure 12 The initial guess (a) and first stage inversion result of the velocity at 1500-th iteration (b) when noises are added to forward modeling data. The density is fixed at constant value for whole modeling region.

(a)

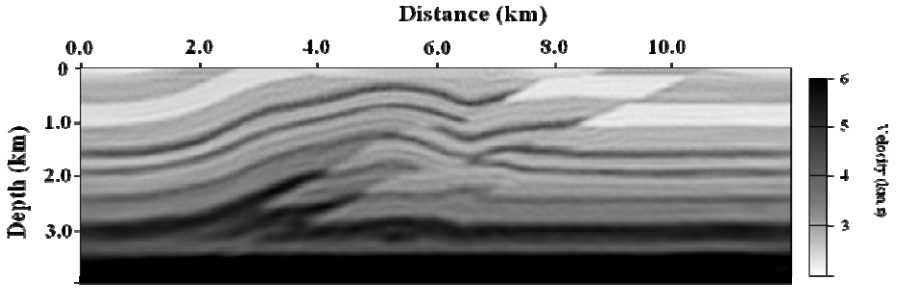

(b)

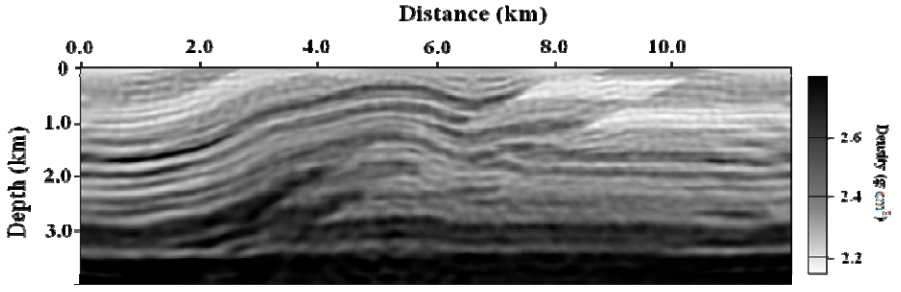

Figure 13 The final results of velocity and density at the 2000-th iteration for (a) P-wave velocity and (b) density when noises are added to forward modeling data.

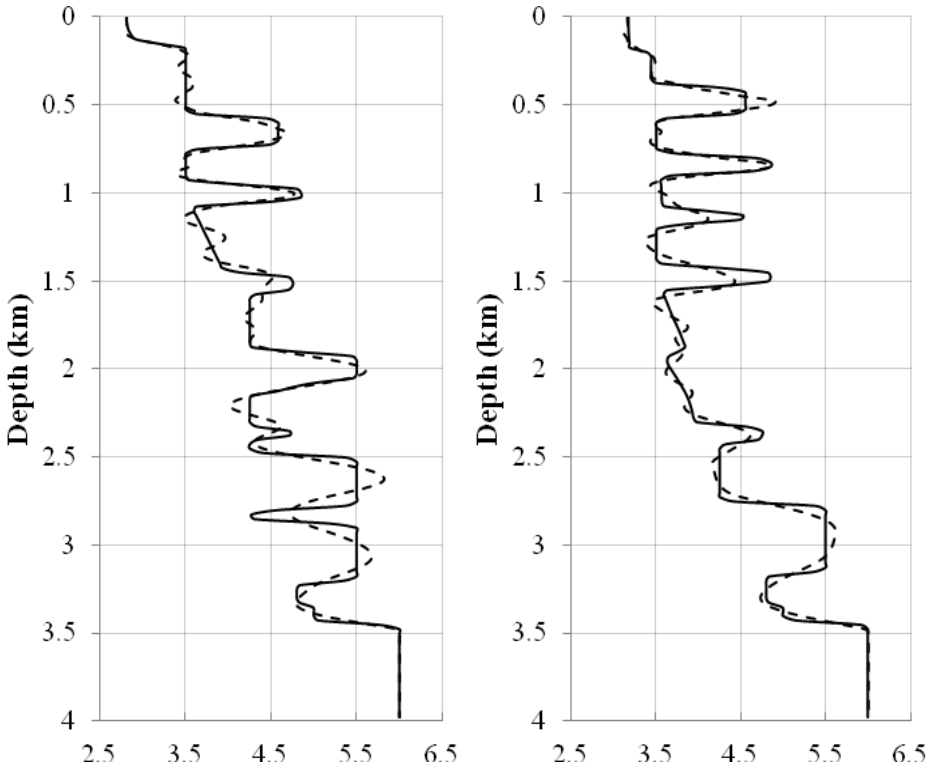

Figure 14 The final inversion results of depth profiles obtained from the velocity model which is shown in Figure 13-(a) at the location of (a) 4km and (b) 6km when noises are added to forward modeling data. Dashed line and black line indicate inverted P-wave velocity and true model. The unit of velocity is km/s.

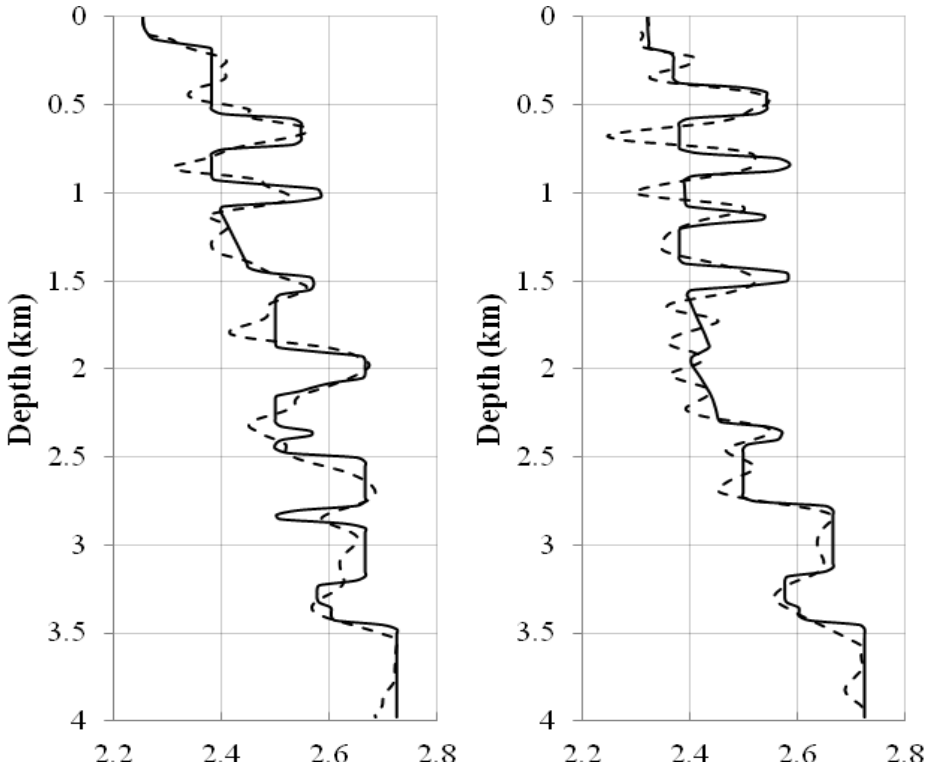

Figure 15 The final inversion results of depth profiles obtained from the density model which is shown in Figure 13-(b) at the location of (a) 4km and (b) 6km when noises are added to forward modeling data. Dashed line and black line indicate inverted the density and true model. The unit of density is g/cm^3.

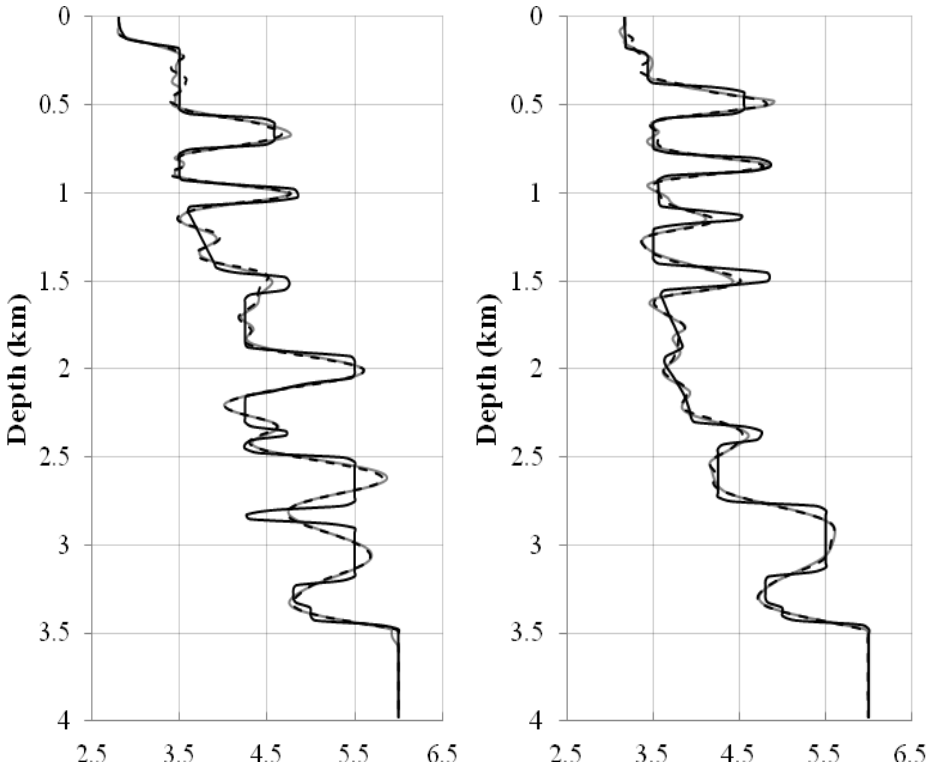

Figure 16 Comparison between depth profiles which are shown in Figure 10 and 14 on P-wave velocity at the location of (a) 4km, and (b) 6km. Dashed line and grey line indicate the case without noises and other case with noises added respectively while black line represents true model.

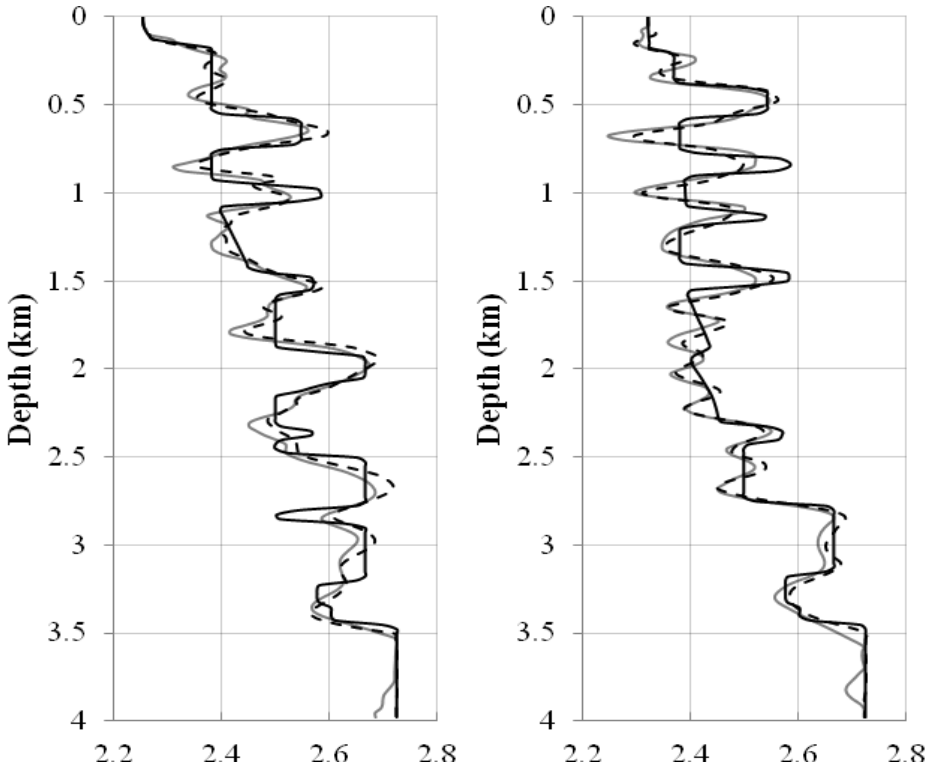

Figure 17 Comparison between depth profiles which are shown in Figure 11 and 15 on density at the location of (a) 4km, and (b) 6km. Dashed line and grey line indicate the case without noises and other case with noises added respectively while black line represents true model.

5. CONCLUSIONS

In acoustic FWI, the velocity has been only reconstructed even though density information is important for geophysical prospecting in estimating the amount of gas and oil precisely and locating reservoir more accurately, particularly through AVO and AVA analyses. Moreover, the density is one of parameters, which is highly difficult to invert properly. For these reasons, we suggest the strategy for acoustic full wavefrom inversion that can reconstruct both velocity and density.

We used two different parameterizations of the acoustic wave equation that consider heterogeneous property of media, while conventional way assumes homogeneous media. One of them is parameterized with the bulk modulus and the density which is called Type-1. The other one is expressed by velocity and density and is called Type-2. From our experiments, Type-1 shows better results for the velocity and Type-2 yields density closer to the true model. From the fact that velocities are generally well reconstructed, we build our inversion strategy over two stages. Velocity is first recovered then velocity and density are inverted simultaneously in second stage with using velocities information obtained in the previous stage. Also, in each stage, we use different parameterization that yields better results on the parameter we focus on. We applied Type-1 in the first stage to invert only the velocity after getting the bulk modulus first and constructing velocity results from the relationship between the bulk modulus and density. Then Type-2 is employed to invert velocity and density while applying the gradient direction of the bulk modulus by chain rule rather than the velocity itself. As a result, we noted that our inversion strategy show better results than conventional way from numerical example of SEG/EAGE ovethrust model. In addition, noise sensitivity test is conducted to investigate the feasibility of the proposed inversion strategy for real field data. Also, l_1-norm objective function is applied because of its robustness for noises. We could see that our inversion strategy still reconstructs velocity and density well when noises are added.

For further study, our inversion strategy has to be conducted on several different geophysical structures with various environmental conditions which can affect inversion results and eventually is needed to be utilized on real field data.

REFERENCES

Davies, Alan. J., 1980, The finite element method: a first approach:Oxford

Fletcher, R., Reeves, C.M., 1964, Function minimized by conjugate gradients: Comput. J., **7**, 149-154.

Forgues E. & Lambaré, G., 1997, Parameterization study for acoustic and elastic ray+Born inversion: J. Seismol. Expl., **6**, 253-277

Gardner, G.H.F., Gardner, L.W. & Gregory, A.R., 1974, Formation velocity and density – diagonostic basis for stratigraphic traps: Geophysics, **39**, 770-780

Ha, T., Y. Choi, C. Shin, and D.-J. Min, 2009, Numerical modeling for 3D acoustic wave equation in the frequency domain: Journal of Seismic Exploration, **18**, 57-79.

Ha, T., W. Chung, and C. Shin, 2009, Waveform inversion using a back-propagation algorithm and a Huber function: Geophysics, **74**, no.3, R15–R24.

Jeong, W., H.-Y., Lee, and D.-J. Min, 2011, Full waveform inversion strategy for density in the frequency domain: Geophys. J. Int., **188**, 1221-1242

Martin G.S., K.J. Marfurt, and S. Larsen, 2002, Marmousi-2: An updated model for the investigation of AVO in structurally complex areas: 72nd Annual International Meeting, SEG, Expanded Abstracts, 1979–1982.

Pratt, R.G., 1999, Seismic waveform inversion in the frequency domain. Part 1:theory and verification in a physical scale model: Geophysics, **64**, 888-901.

Pratt, R.G., and M.H. Worthington, 1990, Inversion theory applied to multi-source crosshole tomography. Part 1: Acoustic wave equation: Geophysical Prospecting, **38**, 287-310.

Pratt, R.G., C. Shin, and G.J. Hicks, 1998, Gauss-Newton and full Newton methods in frequency-space seismic waveform inversion: Geophysical

Journal International, **133**, 341-362.

Pyun, S., W. Son., and C. Shin, 2009, Frequency-domain waveform inversion using an l_1-norm objective function: Exploration Geophysics, **40**, 227-232

Tarantola, A., 1984, Inversion of seismic reflection data in the acoustic approximation: Geophysics, **49**, 1259-1266.

APPENDIX A: JACOBIAN MATRIX TEST

In calculation of vector matrix, the Jacobian matrix is the matrix of first order partial derivatives of function with vector or scalar valued function with respect to another vector. In this way, the Jacobain generalizes the gradient of a scalar value function of multiple variables as in eq. (3). Since we compute the partial derivative wavefields by propagating the virtual source (see eq. (6)), we need to investigate the partial derivative wavefields that is driven by virtual sources (numerical method) are reliable or not by comparing them to ones that are computed by finite difference method (analytic method), which can be expressed as,

$$\frac{\partial \mathbf{u}}{\partial p_k} = \frac{u\left(p_k + \Delta p\right) - u\left(p_k\right)}{\square p},. \tag{A-1}$$

and they should be same in principle.

Semi infinite model is made to perform comparison test between the partial derivative wavefields computed by numerical and analytic methods shown in Figure A1.

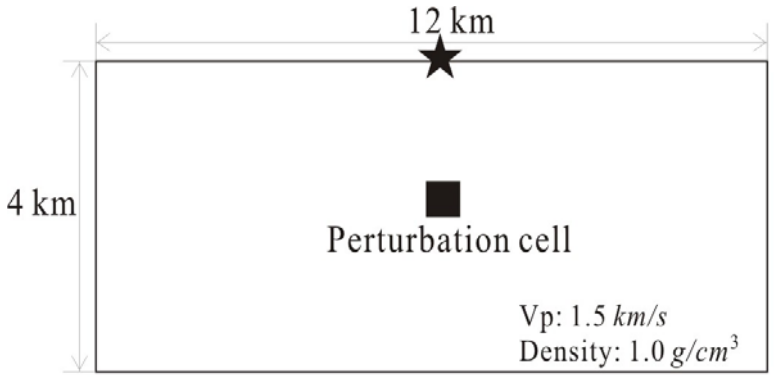

Figure A1 Model for the partial derivatives comparison

The dimension of the model is 12 km × 4 km and a grid interval is 0.025 km. Receivers are placed all nodal points. Seismograms of the partial derivative fields are shown in Figure A2, Figure A3 and Figure A4. Also, traces are extracted at a distance of 4km from the left side in time domain and plotted in

Figure A5 (the bulk modulus), Figure A6 (velocity) and Figure A7 (density). We can see results from numerical and analytic methods are the same with negligible differences. From these observations, the partial derivatives are computed correctly in both cases so that virtual sources that we obtain can be applied in inversion and inversion algorithm is also verified to be right.

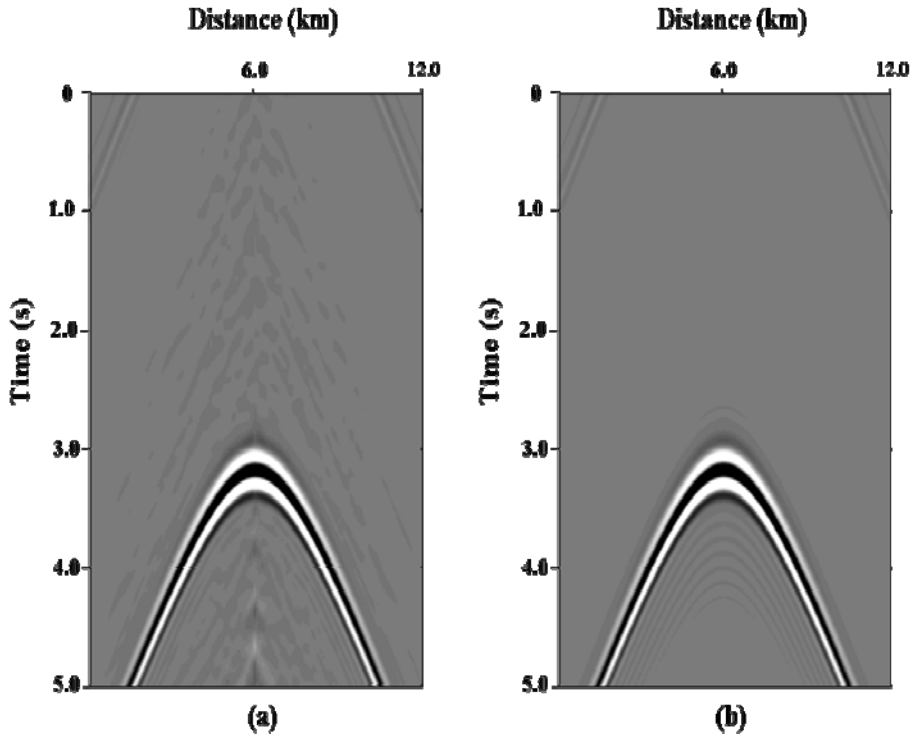

Figure A2 Seismograms of the partial derivative fields obtained by analytic method (a) and numerical method (b) for the bulk modulus.

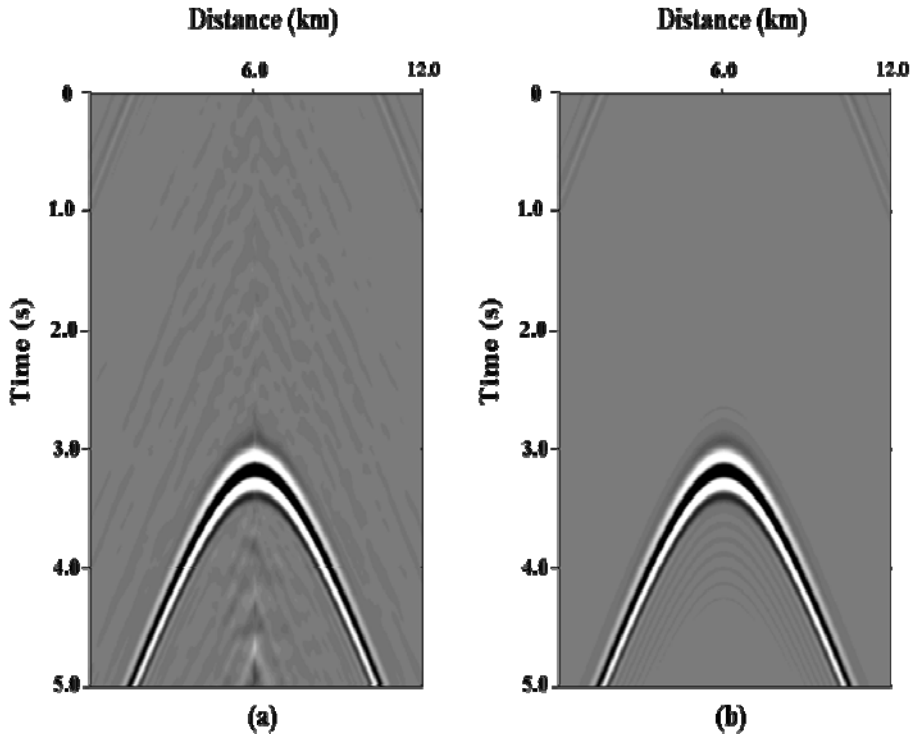

Figure A3 Seismograms of the partial derivative fields obtained by analytic method (a) and numerical method (b) for velocity.

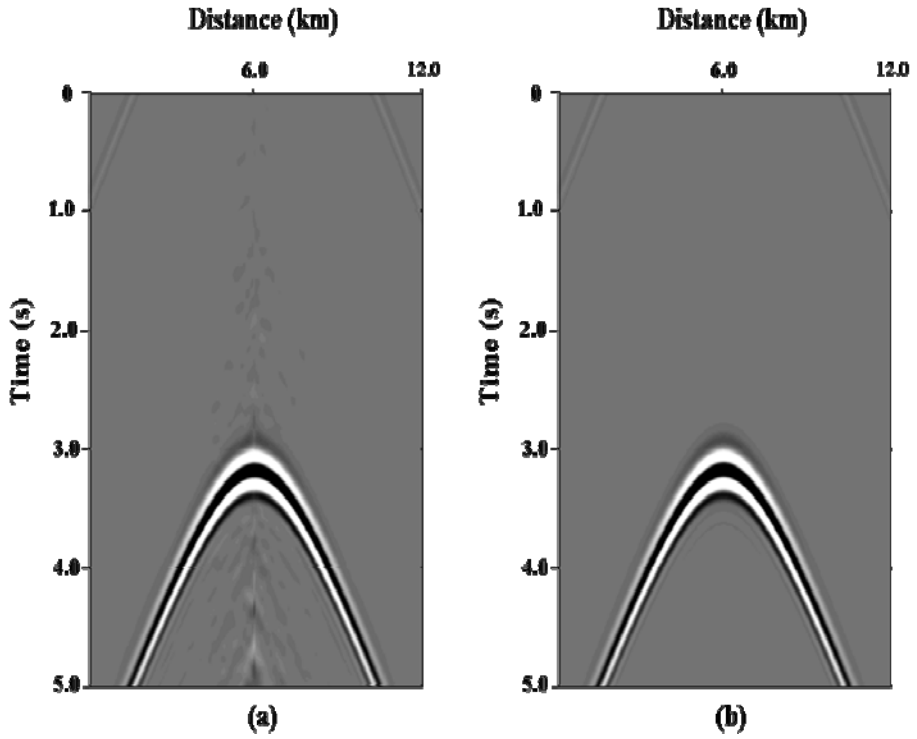

Figure A4 Seismograms of the partial derivative fields obtained by analytic method (a) and numerical method (b) for density.

(a)

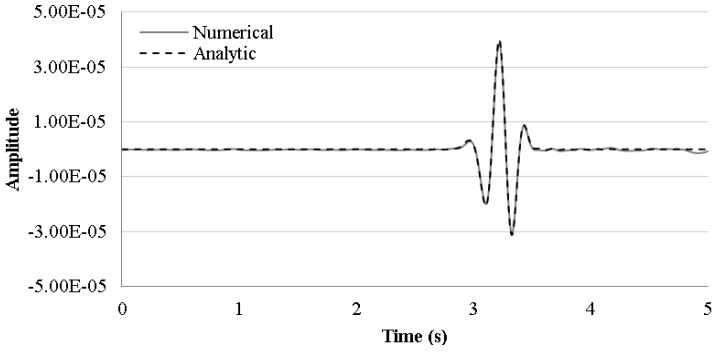

(b)

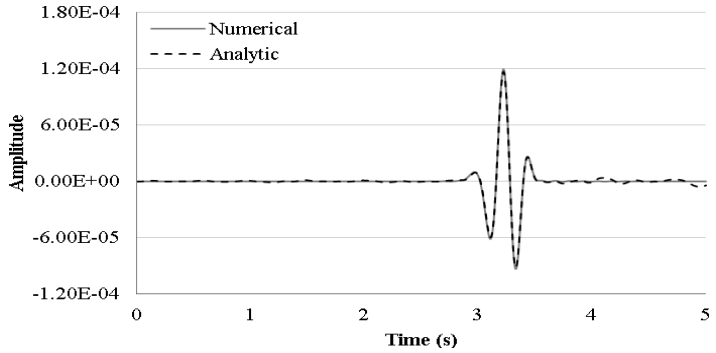

(c)

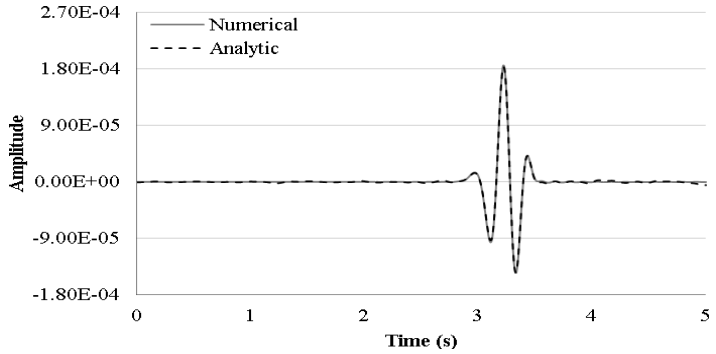

Figure A5 Traces comparisons between numerical and analytic methods in time domain: (a) the bulk modulus, (b) velocity and (c) density.

음향 완전 파형 역산 전략

이 규 화
공과대학 에너지시스템공학부
서울대학교 대학원

완전 파형 역산 기술은 탄성파 자료처리 기법 중 석유 및 가스 부존 가능성이 있는 탐사 지역의 지하 매질의 물성 정보를 이용하여 지하 구조를 영상화하는 유망한 기술 중 하나이다. 최근 들어 여러 가지 물성을 동반하는 탄성 파형 역산에서 좋은 결과를 보여주는 연구 성과들이 나타나고 있지만, 실제 현장 자료에는 현재의 연산 기술 수준과 자료 저장 공간 부족으로 실질적으로 이를 적용할 수 없는 실정이다. 기존의 음향파 완전 파형 역산은 밀도 값이 일정하게 분포한다는 가정을 한 채 주로 P파 속도 정보만을 추정해왔다. 하지만 실제 지하 매질에서 밀도는 일정하게 분포하고 있지 않다. 석유 및 가스 탐사에서 밀도의 중요성이 알려지면서, 밀도 정보를 추정하기 위한 여러 시도들이 있었지만 성공적인 결과를 보여주지 못하였다. 이에 본 논문에서는 l1-norm 목적함수를 이용하면서 속도와 밀도를 동시에 추정할 수 있는 음향파 완전 파형 역산 전략을 제시한다. 역산 전략은 두 가지 단계로 이루어져 있으며 각 단계마다 비균질 매질을 고려한 서로 다르게 매개변수화 된 음향 파동 방정식을 사용한다. 하나는 체적 탄성률과 밀도로 매개변수화 된 Type-1 이며 다른 하나는 속도와 밀도로 이루어진 Type-2 이다. Type-1 은 속도에서 Type-2 는 밀도에서 각각 더 좋은 역산 결과를 보여준다. 이에 역산 첫 번째 단계에서는 밀도는 고정한 채 체적탄성률을 역산한 다음 체적탄성률과 밀도의 관계식을 이용하여 속도 정보를 얻는다. 두 번째 단계에서는 이전 단계에서 얻은 속도 정보를 속도의 초기 모델로 지정하고 속도와 밀도를 동시에 역산한다. 이 때, 속도는 chain rule을 이용하여 체적 탄성률의 최대 급경사 방향을 사용한다. 역산

전략은 잡음이 없는 경우와 추가된 경우 모두에 수행되었다. 합성 자료로는 SEG/EAGE overthrust 모델이 사용되었다. 결과적으로 본 연구에서 제시된 역산 전략을 통해 잡음이 없는 경우와 추가된 경우 모두에서부터 신뢰할 수 있는 수준의 속도와 밀도 정보를 추출할 수 있었다.

주요어: 음향파, 완전 파형 역산, 주파수 영역, 밀도역산
학 번 : 2011-21105